AMERICAN SOCIETY FOR MICROBIOLOGY | mBio®

RESEARCH ARTICLE
Host-Microbe Biology

The Cellular NMD Pathway Restricts Zika Virus Infection and Is Targeted by the Viral Capsid Protein

Krystal A. Fontaine,[a] Kristoffer E. Leon,[a,b] Mir M. Khalid,[a] Sakshi Tomar,[a] David Jimenez-Morales,[a,c*] Mariah Dunlap,[a] Julia A. Kaye,[a] Priya S. Shah,[c*] Steve Finkbeiner,[a,d] Nevan J. Krogan,[a,c] Melanie Ott[a,e]

[a]Gladstone Institutes, San Francisco, California, USA

[b]Medical Scientist Training Program and Biomedical Sciences Graduate Program, University of California, San Francisco, California, USA

[c]Quantitative Biosciences Institute (QBI) and Department of Cellular and Molecular Pharmacology, University of California, San Francisco, California, USA

[d]Departments of Neurology and Physiology, University of California, San Francisco, California, USA

[e]Department of Medicine, University of California, San Francisco, California, USA

ABSTRACT Zika virus (ZIKV) infection of neural progenitor cells (NPCs) *in utero* is associated with neurological disorders, such as microcephaly, but a detailed molecular understanding of ZIKV-induced pathogenesis is lacking. Here we show that *in vitro* ZIKV infection of human cells, including NPCs, causes disruption of the nonsense-mediated mRNA decay (NMD) pathway. NMD is a cellular mRNA surveillance mechanism that is required for normal brain size in mice. Using affinity purification-mass spectrometry, we identified multiple cellular NMD factors that bind to the viral capsid protein, including the central NMD regulator up-frameshift protein 1 (UPF1). Endogenous UPF1 interacted with the ZIKV capsid protein in coimmunoprecipitation experiments, and capsid expression posttranscriptionally downregulated UPF1 protein levels, a process that we confirmed occurs during ZIKV infection. Cellular fractionation studies show that the ZIKV capsid protein specifically targets nuclear UPF1 for degradation via the proteasome. A further decrease in UPF1 levels by RNAi significantly enhanced ZIKV infection in NPC cultures, consistent with a model in which NMD restricts ZIKV infection in the fetal brain. We propose that ZIKV, via the capsid protein, has evolved a strategy to lower UPF1 levels and dampen antiviral activities of NMD, which in turn contributes to neuropathology *in vivo*.

IMPORTANCE Zika virus (ZIKV) is a significant global health threat, as infection has been linked to serious neurological complications, including microcephaly. Using a human stem cell-derived neural progenitor model system, we find that a critical cellular quality control process called the nonsense-mediated mRNA decay (NMD) pathway is disrupted during ZIKV infection. Importantly, disruption of the NMD pathway is a known cause of microcephaly and other neurological disorders. We further identify an interaction between the capsid protein of ZIKV and up-frameshift protein 1 (UPF1), the master regulator of NMD, and show that ZIKV capsid targets UPF1 for degradation. Together, these results offer a new mechanism for how ZIKV infection can cause neuropathology in the developing brain.

KEYWORDS Zika virus, nonsense-mediated mRNA decay pathway, virus-host interactions

Zika virus (ZIKV) is a mosquito-borne RNA virus that belongs to the *Flaviviridae* family. First isolated in Uganda in 1947, ZIKV remained relatively obscure for decades following its discovery because infection was associated with only mild

Received 25 September 2018 **Accepted** 28 September 2018 **Published** 6 November 2018

Citation Fontaine KA, Leon KE, Khalid MM, Tomar S, Jimenez-Morales D, Dunlap M, Kaye JA, Shah PS, Finkbeiner S, Krogan NJ, Ott M. 2018. The cellular NMD pathway restricts Zika virus infection and is targeted by the viral capsid protein. mBio 9:e02126-18. https://doi.org/10.1128/mBio.02126-18.

Editor Jaisri R. Lingappa, University of Washington

Address correspondence to Melanie Ott, melanie.ott@gladstone.ucsf.edu.

* Present address: David Jimenez-Morales, Department of Medicine, Stanford University, Stanford, California, USA; Priya S. Shah, Departments of Chemical Engineering and Microbiology and Molecular Genetics, University of California, Davis, California, USA.

K.A.F and K.E.L contributed equally to this work.

This article is a direct contribution from a Fellow of the American Academy of Microbiology. Solicited external reviewers: Peter Sarnow, Stanford University School of Medicine; Scott Michael, Florida Gulf Coast University.

disease. However, more severe clinical manifestations, including microcephaly, have been observed during the recent spread of ZIKV through the Americas (1). ZIKV infection induces cell cycle arrest and apoptosis in neural progenitor cells (NPCs) in *in vitro* studies and *in vivo* mouse models, with the latter resulting in cortical thinning and microcephaly (2–6). While it is now established that ZIKV infection during pregnancy is a causative agent of microcephaly (7), the molecular mechanisms underlying ZIKV-induced neuropathogenesis remain largely unknown.

Similar to other flaviviruses, ZIKV contains a single-stranded, positive-sense RNA genome of ~11 kb in size. The genome encodes a single polyprotein that is posttranslationally processed by both host and viral proteases to produce 3 structural proteins and 7 nonstructural proteins (8, 9). The flavivirus capsid, which is the first protein encoded in the genome, is a major structural element required for the encapsidation of the RNA genome during virion assembly (10). While flavivirus replication is known to occur in the cytoplasm, a significant portion of the viral capsid protein localizes to the nucleus during infection (10, 11). Although the role of nuclear capsid during infection is less clear, several functions have been suggested. The capsid protein from dengue virus, a close relative of ZIKV, binds to core histones and inhibits nucleosome formation, thus implicating the protein in altering host gene expression (12). Furthermore, several flavivirus capsid proteins, including ZIKV capsid, localize to the nucleolus, with many interacting with nucleolar proteins to promote viral particle production (13–16).

The nonsense-mediated mRNA decay (NMD) pathway was initially discovered as a highly conserved quality control system that destroys transcripts containing premature termination codons (PTCs) (17). Following splicing of pre-mRNAs, a multisubunit protein complex called the exon-junction complex (EJC) is deposited onto mRNAs near the sites of exon-exon junctions. If a PTC is found ~50 to 55 nucleotides upstream of an EJC, the mRNA will be subjected to NMD-mediated degradation initiated by the recruitment of the RNA helicase up-frameshift protein 1 (UPF1). UPF1 plays a central role in the NMD pathway by linking the translation termination event to the assembly of a surveillance complex, resulting in NMD activation (18). Interestingly, microcephaly has been associated with genetic mutations that result in the impairment of the NMD pathway. While knockout of *Upf1* and other NMD factors is embryonic lethal in mice (19), mice haploinsufficient for the EJC components *Magoh*, *Rbm8a*, and *Eif4a3* exhibit aberrant neurogenesis and microcephaly (20–22).

In addition to PTC-containing transcripts, it is now known that the NMD pathway recognizes a broader range of RNA substrates. Notably, the NMD controls the "normal" expression of ~10% of the cellular transcriptome and is regarded as a posttranscriptional mechanism of gene regulation (23). Furthermore, the NMD pathway also regulates viral infections. While it was first reported that UPF1 promotes the infectivity of HIV-1 progeny virions (24), replication of several human RNA viruses, including human T-cell lymphotropic virus type 1 (HTLV-1), Semliki Forest virus, and Sindbis virus, is enhanced following UPF1 knockdown, implicating UPF1 and the NMD pathway, either directly or indirectly, in the host antiviral response (25–28). As ZIKV infection and NMD impairment both promote microcephaly development, and we previously described disruption of the NMD pathway in cells infected with a related flavivirus, the hepatitis C virus (HCV) (29), we hypothesized that ZIKV infection manipulates the cellular NMD pathway, a process contributing to ZIKV-induced neuropathology.

RESULTS

The NMD pathway is impaired during ZIKV infection. To determine whether ZIKV infection affects NMD, we infected human hepatoma cells (Huh7) and human induced pluripotent stem cell (iPSC)-derived NPCs with ZIKV for 48 h. We isolated total RNA from infected cells and measured mRNA levels of three canonical NMD substrates: asparagine synthetase (ASNS), cysteinyl-tRNA synthetase (CARS), and SR protein SC35 (29). ASNS, CARS, and SC35 transcripts were significantly elevated in Huh7 cells and NPCs following infection with Asian lineage ZIKV strain P6-740 (Fig. 1a). Levels of NMD substrates were also elevated in Huh7 cells infected with the contemporary ZIKV clinical

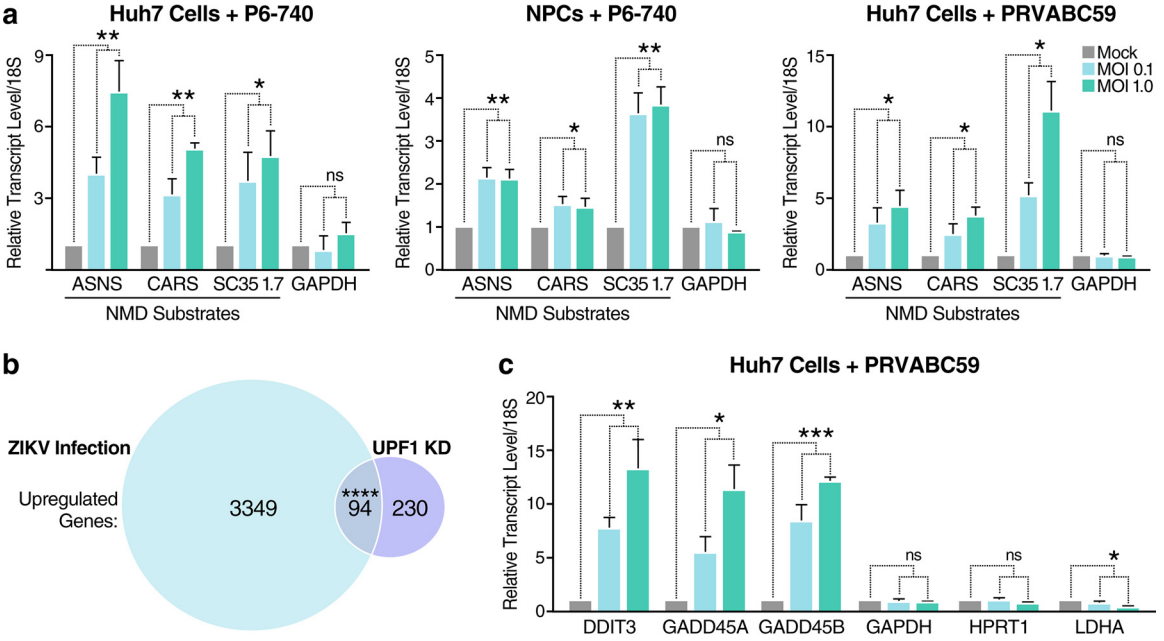

FIG 1 ZIKV infection disrupts the NMD pathway. (a) Transcript levels of NMD substrates and a housekeeping gene control from Huh7 cells or NPCs mock infected or infected with ZIKV strain P6-740 or the contemporary clinical isolate PRVABC59. Cells were infected at a multiplicity of infection (MOI) of 0.1 or 1 and harvested at 48 hours postinfection (hpi). Data are represented as means plus standard errors of the means (SEM) (error bars). Statistical significance (and *P* values) were calculated by unpaired Student's *t* test and indicated as follows: *, $P \leq 0.05$; **, $P \leq 0.01$; ns, not significant. Three independent experiments were performed. (b) Venn diagram showing overlap of significantly upregulated genes associated with ZIKV infection of NPCs and UPF1 knockdown (KD) in HeLa cells. RNA-Seq analyses of mock-infected or ZIKV-infected NPCs harvested at 56 hpi and control siRNA-treated or UPF1 siRNA-treated HeLa TO cells harvested at 72 h posttransfection (hpt). The GeneProf hypergeometric probability calculator was then used to generate a hypergeometric *P* value. ****, $P \leq 0.0001$. (c) Transcript levels of housekeeping genes and select genes involved in cell cycle arrest and apoptosis that were identified in panel b. Huh7 cells were mock infected or infected with ZIKV PRVABC59 at an MOI of 0.1 or 1 and harvested at 48 hpi. Data are represented as means plus SEM. The *P* values were calculated by unpaired Student's *t* test. *, $P \leq 0.05$; **, $P \leq 0.01$; ***, $P \leq 0.001$; ns, not significant. $n = 3$ independent experiments.

isolate PRVABC59 (Puerto Rico, 2015) (Fig. 1a). We found that the ZIKV-induced increase in NMD transcripts did not reflect a global increase in transcription, as mRNA levels of housekeeping genes, including glyceraldehyde 3-phosphate dehydrogenase (GAPDH), were not altered in infected cells (Fig. 1a). Together, these results indicate that the NMD pathway is impaired in ZIKV-infected cells.

NMD substrates are regulated through the ATP-dependent RNA helicase activity of UPF1, the central regulator of NMD (18). To determine whether ZIKV infection broadly affects NMD, we utilized two publicly available RNA sequencing (RNA-Seq) data sets to compare genome-wide transcriptional alterations found during ZIKV infection (6) to those found following UPF1 knockdown (30). As shown in Fig. 1b, there is a significant overlap in upregulated genes between these two data sets. Interestingly, several of the overlapping genes are canonical NMD substrates (31–35) involved in cell cycle arrest and induction of apoptosis, two conditions linked to ZIKV-associated neuropathology (5). These genes include DNA damage-inducible transcript 3 (DDIT3) (36) and growth arrest and DNA damage-inducible protein 45 alpha and beta (GADD45A and GADD45B, respectively) (37). Via quantitative real-time reverse transcription-PCR (qRT-PCR), we confirmed that transcripts of each were upregulated following infection of Huh7 cells with ZIKV PRVABC59, while the mRNA levels of the housekeeping genes GAPDH, hypoxanthine phosphoribosyltransferase 1 (HPRT1), and lactate dehydrogenase A (LDHA) were not elevated (Fig. 1c). Combined, these data show that ZIKV infection is associated with dysregulated expression of NMD substrates relevant to ZIKV-mediated neuropathogenesis.

ZIKV capsid interacts with the NMD pathway. We previously showed that the core protein of HCV, as well as the capsid protein of the related flaviviruses dengue

virus and West Nile virus, interact with the host protein within bgcn homolog (WIBG/PYM1), an EJC disassembly factor associated with NMD (29, 38). To examine potential interactions between ZIKV and the NMD pathway, we separately analyzed data generated from an affinity purification-mass spectrometry (AP-MS) screen to specifically query whether the capsid protein of ZIKV interacts with NMD-associated host factors (P. S. Shah et al., submitted for publication). ZIKV-host protein-protein interaction (PPI) maps were generated in HEK293T cells using ZIKV proteins from the Ugandan 1947 strain MR 766 or the French Polynesian 2013 strain H/PF/2013 as bait proteins.

From this analysis, we found that ZIKV capsid proteins interacted with several components of the NMD pathway, including multiple members of the EJC complex, as well as UPF1 and UPF3B, the latter an NMD effector that stimulates UPF1 helicase activity (Fig. 2a) (39). Importantly, the NMD host factors that interacted with each of the two different capsid proteins greatly overlapped, revealing that the interaction between capsid and the NMD pathway is conserved across the Asian and African lineages of ZIKV (Fig. 2a). Next, we validated the binding of ZIKV capsid to select NMD host factors by coimmunoprecipitating FLAG-tagged capsid protein with endogenous UPF3B or UPF1 in HEK293T cells. Both UPF3B and UPF1 proteins coimmunoprecipitated with ZIKV capsid, thus confirming the AP-MS results (Fig. 2b and c, respectively). UPF1 interacted with the viral capsid protein independently from its RNA-binding and ATPase/helicase capacities, as ZIKV capsid coimmunoprecipitated with UPF1 mutants deficient in these functions following overexpression (Fig. 2d).

ZIKV capsid degrades UPF1, the master regulator of NMD. Surprisingly, we consistently observed a decrease in UPF1, but not UPF3B, protein levels in the input lysate of ZIKV capsid-transfected cells, pointing to a specific perturbation of endogenous UPF1 expression by ZIKV capsid (Fig. 2c). To confirm that UPF1 protein levels are dysregulated during ZIKV infection, we performed Western blot analysis of infected Huh7 cells and NPCs. Cellular UPF1 protein levels were consistently downregulated by ~50% in ZIKV-infected Huh7 cells, whereas an ~25% reduction was observed in ZIKV-infected NPCs (Fig. 2e), mirroring the difference in infection efficiencies achieved in these two cell systems. UPF1 transcript levels were not decreased in ZIKV-infected cells or following ZIKV capsid overexpression, indicating that UPF1 is posttranscriptionally downregulated during ZIKV infection (see Fig. S1a and b, respectively, in the supplemental material).

Because ZIKV capsid and UPF1 both localize to the nucleus and the cytoplasm (13, 40), we performed fractionation studies in ZIKV capsid-transfected HEK293T cells to determine whether UPF1 is downregulated within a specific cellular compartment. Capsid expression markedly decreased nuclear UPF1 levels, whereas cytoplasmic levels were unchanged (Fig. 3a). We next examined a potential role for the autophagic and proteasomal pathways, both of which are known to mediate nuclear protein degradation, in ZIKV capsid-induced UPF1 downregulation. As shown in Fig. S2, nuclear UPF1 levels in ZIKV capsid-transfected cells were not rescued by inhibition of cellular autophagy via bafilomycin A1 treatment. However, nuclear UPF1 levels were restored in a dose-dependent manner following treatment with the proteasome inhibitor bortezomib (Fig. 3b), indicating enhanced proteasomal degradation of nuclear UPF1 in the presence of ZIKV capsid. Although ZIKV capsid colocalized with endogenous UPF1 in the cytoplasm of transfected Huh7-Lunet cells (Mander's colocalization coefficient of ~57%), we detected very little colocalization within the nucleus (~7%) (Fig. S3). We hypothesized that this was due to specific degradation of UPF1 by ZIKV capsid in the nucleus. Indeed, when cells were treated with bortezomib, the fraction of nuclear UPF1 colocalizing with ZIKV capsid increased ~8-fold, while the fraction of nuclear capsid interacting with UPF1 remained unchanged (Fig. 3c). These results demonstrate that ZIKV capsid interacts with UPF1 both in the cytoplasm and nucleus but that it specifically targets nuclear UPF1 for proteasomal degradation.

UPF1 is a restriction factor of ZIKV. To test the effect of lowered UPF1 levels on ZIKV infection, we further decreased UPF1 expression prior to ZIKV infection by

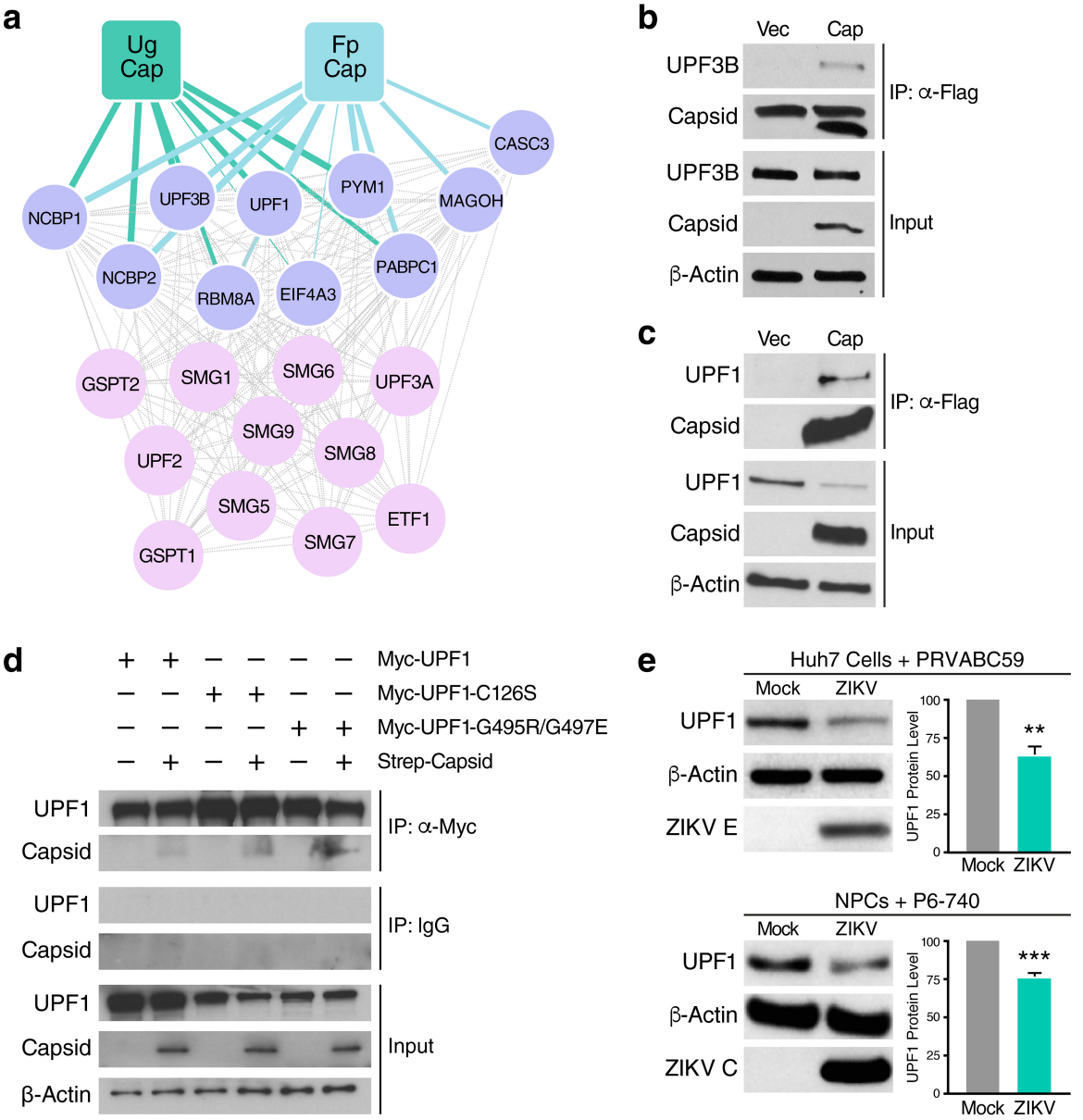

FIG 2 The capsid protein of ZIKV interacts with the NMD pathway. (a) Ugandan ZIKV capsid (Ug Cap) (MR 766) and French Polynesian ZIKV capsid (Fp Cap) (H/PF/2013) PPI maps that show significant enrichment for host NMD-associated factors (purple), as identified by AP-MS (SAINTq probability score of $>$ 0.9 and false-discovery rate [FDR] of $<$0.05). Ten interactions between Fp Cap and host NMD factors (hypergeometrical test, P value $= 7.16 \times 10^{-10}$) and eight interactions between Ug Cap and host NMD factors (P value $= 3.45 \times 10^{-7}$) were identified. (b) Coimmunoprecipitation (co-IP) and Western blot analysis of HEK293T cells transfected with vector or Flag-tagged ZIKV capsid (H/PF/2013, Asian lineage) and harvested at 48 hpt to immunoprecipitate endogenous UPF3B. The upper band detected in the IP Capsid blot represents a nonspecific artifact. α-Flag, anti-Flag antibody. (c) Co-IP and Western blot analysis of HEK293T cells transfected with vector or Flag-tagged ZIKV capsid and harvested at 48 hpt to immunoprecipitate endogenous UPF1. (d) Myc tag co-IP and Western blot analysis of HEK293T cells transfected with Strep-tagged ZIKV capsid and Myc-UPF1 (wild type), Myc-UPF1-C126S (RNA-binding mutant) or Myc-UPF1-G495R/G497E (ATPase/helicase mutant) and harvested at 48 hpt to immunoprecipitate ZIKV capsid. (e) Western blot analysis of UPF1 levels in mock-infected and ZIKV-infected (PRVABC59, MOI of 1) Huh7 cells or mock-infected and ZIKV-infected (P6-740, MOI of 1) NPCs harvested at 48 hpi, with β-actin and ZIKV envelope (ZIKV E) or ZIKV capsid (ZIKV C) protein serving as loading and infection controls, respectively. Densitometric analyses were performed using ImageJ to quantify relative band intensities. Data are represented as means plus SEM. The P values were calculated by unpaired Student's t test. **, $P \leq 0.01$; ***, $P \leq 0.001$. $n = 3$ independent experiments.

transfecting NPCs with either nontargeting siRNA or a pool of UPF1-specific siRNAs. We then infected the transfected cells with ZIKV and measured viral RNA levels, as well as infectious titers, 48 h postinfection (hpi). UPF1 knockdown was successful in siRNA-treated cells, as confirmed by Western blot analysis (Fig. 4a). The depletion of UPF1 in NPCs prior to infection resulted in a significant increase in both ZIKV RNA levels and

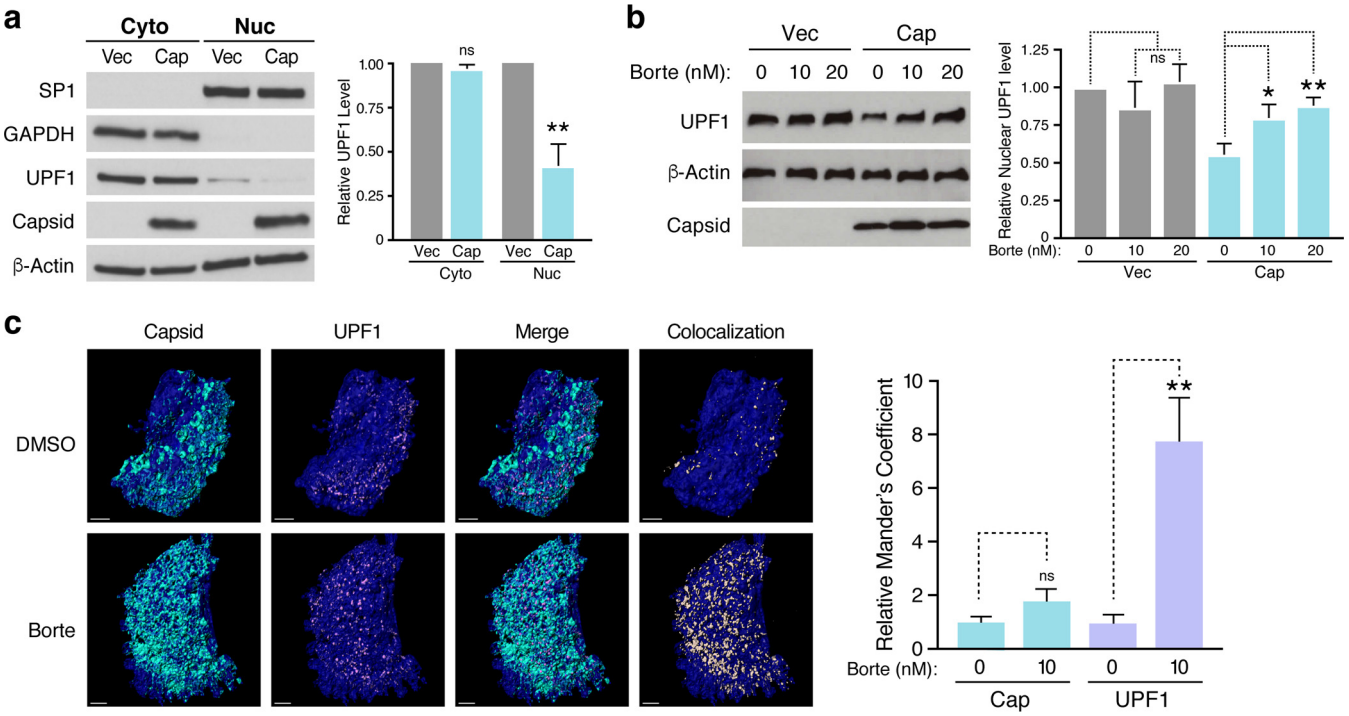

FIG 3 ZIKV capsid degrades UPF1, the master regulator of NMD, via a proteasome-dependent mechanism. (a) Western blot analysis of UPF1 levels in subcellular fractionated HEK293T cells transfected with vector or Flag-tagged ZIKV capsid (H/PF/2013, Asian lineage) for 48 h. GAPDH was used as a cytoplasmic marker, and SP1 was used as a nuclear marker to ensure optimal fractionation. Densitometric analyses were performed using ImageJ to quantify relative band intensities. Data are represented as means plus SEM. *P* values were calculated by unpaired Student's *t* test. **, $P \leq 0.01$; ns, not significant. $n = 3$ independent experiments. (b) Western blot analysis of nuclear UPF1 levels in fractionated HEK293T cells transfected with vector or Flag-tagged ZIKV capsid for 48 h. Cells were treated with DMSO or increasing concentrations of the proteasome inhibitor bortezomib (Borte) for 24 h before harvest. Densitometric analyses were performed using ImageJ to quantify relative band intensities. Data are represented as means plus SEM. *P* values were calculated by one-way ANOVA with multiple comparisons. *, $P \leq 0.05$; ns, not significant. $n = 3$ independent experiments. (c) Representative 3D confocal microscopy images of the nuclei of Huh7-Lunet cells transfected with Strep-tagged ZIKV capsid. Cells were treated at 24 hpt with DMSO or 10 nM bortezomib and processed for immunostaining at 48 hpt with antibodies against Strep tag (turquoise) and endogenous UPF1 (purple). DAPI (blue) was used to stain and define the nuclei. Each channel was reconstructed digitally for visualization of the 3D colocalization. The thresholded Mander's correlation coefficients were determined, and *P* values were calculated by unpaired Student's *t* test. **, $P \leq 0.01$. $n = 8$ cells per condition. Scale bars represent 3 μm.

infectious virus production (Fig. 4b and c, respectively), indicating that expression of UPF1 restricts ZIKV infection at or before the RNA replication stage. To differentiate between these two stages, we analyzed double-stranded RNA (dsRNA) intermediates representing presumed viral RNA replication centers in infected NPCs (Fig. 4d) (41). Using confocal microscopy and 3D reconstruction analyses, we observed no significant difference in the number and size of dsRNA foci per cell when comparing ZIKV-infected, UPF1-depleted NPCs to ZIKV-infected cultures expressing UPF1 (Fig. 4e and f). Instead, we found a significant increase in the number of infected cells in NPC cultures when UPF1 was depleted, indicating that UPF1 regulates permissivity of NPCs to ZIKV infection at an early stage prior to viral RNA replication (Fig. 4g).

DISCUSSION

In summary, we identified the NMD pathway as a restriction mechanism for ZIKV infection in human NPCs. NMD was partially inactivated in ZIKV-infected NPCs through expression of the viral capsid protein and the resulting degradation of host nuclear UPF1. As further weakening NMD by depleting UPF1 resulted in a marked increase in the number of infected cells, we propose a model in which an evolutionary "arms race" between cellular NMD and ZIKV determines whether a cell is successfully infected (Fig. 4h).

Downregulation of UPF1 by ZIKV capsid is not complete and is likely limited by the damaging effects of NMD disruption, as illustrated by the upregulation of genes involved in cell growth arrest and apoptosis. Indeed, knockout of *Upf1* and other

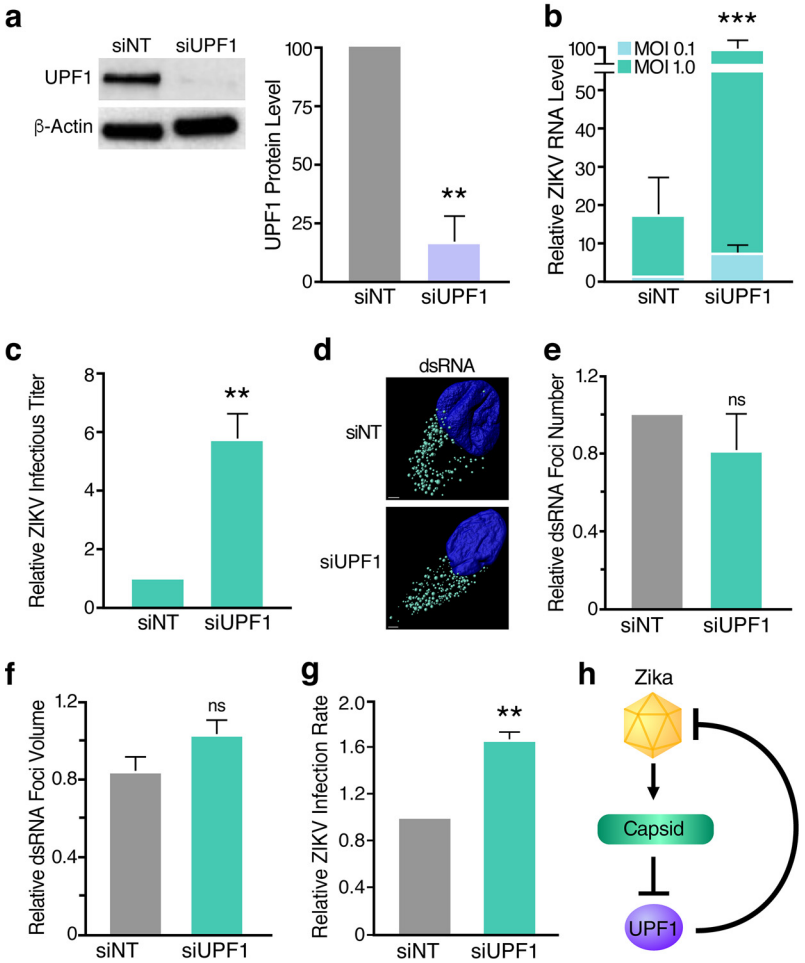

FIG 4 UPF1 knockdown enhances the permissivity of NPCs to ZIKV infection. (a) Western blot analysis of UPF1 levels in NPCs transfected with nontargeting siRNA (siNT) or a pool of UPF1-specific siRNAs (siUPF1) at 96 hpt. Densitometric analyses were performed using ImageJ to quantify relative band intensities. Data are represented as means plus SEM. *P* values were calculated by unpaired Student's *t* test. **, $P \leq 0.01$. $n = 3$ independent experiments using one NPC line. (b) ZIKV RNA levels in siNT-treated or siUPF1-treated NPCs infected with ZIKV strain PRVABC59 at an MOI of 0.1 or 1 and harvested at 48 hpi. Data are represented as means plus SEM. *P* values were calculated by two-tailed ratio paired Student's *t* test. ***, $P \leq 0.001$. $n = 3$ independent experiments using one NPC line. (c) Released infectious virus from siNT-treated or siUPF1-treated, ZIKV-infected (MOI of 1) NPCs harvested at 48 hpi. Data are represented as means plus SEM. *P* values were calculated by unpaired Student's *t* test. **, $P \leq 0.01$. $n = 3$ independent experiments using one NPC line. (d) Representative confocal microscopy images of a ZIKV-infected, siNT-treated NPC or a ZIKV-infected, siUPF1-treated NPC with the nuclei stained with DAPI (blue) and ZIKV dsRNA foci stained with the anti-dsRNA mAb J2 (teal). 3D image rendering and reconstructed dsRNA foci were produced using the Imaris spot detection function. The scale bars represent 2 μm. (e) Number of dsRNA foci was averaged for each cell. Data are represented as means plus SEM. *P* values were calculated by two-tailed ratio paired Student's *t* test. ns, not significant. $n = 3$ independent experiments using two NPC lines, with 3 to 10 cells analyzed per condition for each experiment. (f) Measurements of dsRNA focus volume were averaged for each cell. Data are represented as means plus SEM. *P* values were calculated by two-tailed ratio paired Student's *t* test. ns, not significant. $n = 3$ independent experiments using two NPC lines, with 3 to 10 cells analyzed per condition for each experiment. (g) Infection rates of siNT-treated or siUPF1-treated, ZIKV-infected (MOI of 1) NPCs measured at 48 hpi. Fixed cells were subjected to the anti-DENV mAb 1.6D, which also recognizes the ZIKV envelope protein (56). Data are represented as means plus SEM. *P* values were calculated by two-tailed ratio paired Student's *t* test. **, $P \leq 0.01$. $n = 3$ independent experiments using two NPC lines. (h) Model of the interaction between the capsid protein of ZIKV and UPF1 of the NMD pathway.

members of the NMD pathway is embryonic lethal in mice (19). However, mice haploinsufficient for NMD factors upstream of UPF1, including *Magoh*, *Rbm8a*, and *Eif4a3*, develop microcephaly (20–22). Thus, the reduction in nuclear UPF1 we observe in ZIKV-infected NPCs could contribute to the microcephaly phenotype caused by ZIKV

infection in the fetal brain. While fetal and adult NPCs appear to be transcriptionally distinct (42), it has been shown that adult NPCs are also permissive to ZIKV infection (43). As the NMD pathway is a ubiquitous cellular surveillance mechanism, it is likely that ZIKV capsid targets UPF1 for degradation in any cell type that is susceptible to ZIKV infection. Accordingly, we have found that UPF1 is degraded following infection of both NPCs and hepatic Huh7 cells.

Why ZIKV capsid specifically downregulates nuclear UPF1 and how nuclear UPF1 contributes to ZIKV restriction remain unanswered. Several studies suggest that NMD is associated with the nucleus, although this issue remains controversial. Multiple transcripts, such as those encoding T cell receptor beta, triosephosphate isomerase, and mouse major urinary protein, have been shown to be specifically degraded in purified nuclei or reduced in nuclear fractions (44). These data support the model that selectively depleting nuclear UPF1 levels disrupts NMD function in ZIKV-infected cells. In addition, UPF1 is involved in several other processes within the nucleus, including nucleus-associated RNA metabolism, cell cycle progression, and DNA replication (40). Therefore, by targeting nuclear UPF1, ZIKV could disrupt these processes and program target cells for viral replication. Notably, viral RNA replication is thought to occur solely within the cytoplasmic compartment (45, 46). Using confocal microscopy and 3D reconstruction, we did not detect dsRNA foci localized within the nuclei of ZIKV-infected cells (data not shown), supporting our finding that UPF1 does not restrict viral RNA replication. While our results suggest a role for nuclear UPF1 in ZIKV restriction, it is possible that UPF1 also serves as a restriction factor of ZIKV within the cytoplasm. Previously, it was shown that UPF1 suppresses alphavirus replication by degrading the incoming viral RNA following uncoating in the cytosol (28). Thus, ZIKV may possess an additional mechanism to prevent cytoplasmic UPF1 from targeting its incoming RNA genome for destruction.

Our data reveal that nuclear UPF1 is degraded by ZIKV capsid in a proteasome-dependent manner. While the nuclear proteasome has not been specifically linked to microcephaly, it plays critical roles in the regulation of chromatin structure, gene expression, DNA repair, and protein quality control (47). Thus, the co-opting of the nuclear proteasome by ZIKV capsid to degrade UPF1 could disrupt its normal proteasomal activity and further contribute to the cytopathic effects associated with ZIKV infection. Furthermore, given that the capsid protein of the closely related dengue virus can translocate across cell membranes (48), it is possible that capsid released from apoptotic, ZIKV-infected cells can enter neighboring, uninfected cells to degrade UPF1, thus increasing permissivity of bystander cells to ZIKV infection. Studies are ongoing to determine the precise molecular mechanism of ZIKV capsid-mediated UPF1 degradation and how UPF1 depletion enhances ZIKV replication, directly or indirectly. Ultimately, these data may help inform new therapeutic approaches, as reinforcement of the antiviral properties of the NMD pathway is expected to enhance resistance of NPCs to ZIKV infection and to promote normal neurodevelopment in infected fetuses.

MATERIALS AND METHODS

Viruses and cells. Two Asian lineage strains of ZIKV, P6-740 (ATCC VR-1845) and PRVABC59 (ATCC VR-1843), were used for all experiments. ZIKV stocks were propagated in Vero cells (ATCC), and titers were determined by plaque assays on Vero cells. Huh7 cells (ATCC), Huh7-Lunet cells (Ralf Bartenschlager, Heidelberg University), and Vero cells were maintained in Dulbecco's modified Eagle's medium (DMEM) with 10% fetal bovine serum (FBS), 2 mM L-glutamine, 100 U/ml penicillin, and 100 μg/ml streptomycin. HEK293T cells (ATCC) were maintained in DMEM/H21 medium supplemented with 10% FBS, 100 U/ml penicillin, 100 μg/ml streptomycin, and 1 mM sodium pyruvate or DMEM with 10% FBS, 2 mM L-glutamine, 100 U/ml penicillin, and 100 μg/ml streptomycin. Human iPSC-derived NPCs were generated and maintained as described previously (49). All of the human fibroblast cell lines used to generate iPSCs came from the Coriell Institute for Medical Research and Yale Stem Cell Center. The iPSCs used in these studies were the CTRL2493nXX, CS2518nXX, and Cs71iCTR-20nXX lines. CTRL2493nXX was derived from the parental fibroblast line ND31845 that was biopsied from a healthy female at 71 years of age. CS2518nXX was derived from the parental fibroblast line ND30625 that was biopsied from a healthy male at 76 years of age. CS71iCTR-20nXX was derived from the parental fibroblast line ND29971 that was biopsied from a female at 61 years of age. For virus infections, NPCs plated on Matrigel-coated

(Corning) multiwell plates or Huh7 cells were infected with ZIKV at a multiplicity of infection (MOI) of 0.1 or 1 for 2 h at 37°C. Infected cells were harvested at 48 hpi for all analyses.

Affinity purification, mass spectrometry, and AP-MS scoring. The ZIKV capsid open reading frames (ORFs) from the Ugandan 1947 strain MR 766 or the French Polynesian 2013 strain H/PF/2013 were cloned into pCDNA4_TO with a C-terminal 2xStrep II affinity tag for expression in human cells. The viral capsid proteins (three biological replicates), as well as GFP (two biological replicates) and empty vector (ten biological replicates) as negative controls, were expressed in HEK293T cells, and affinity purifications were performed as previously described (50). Briefly, clarified lysates were incubated with Strep-Tactin Superflow (IBA) overnight at 4°C. Proteins were eluted with 50 mM Tris (pH 7.5), 150 mM NaCl, and 1 mM EDTA containing 2.5 mM Desthiobiotin (IBA) for 30 min at 4°C. Lysates and affinity-purified eluates were analyzed by Western blotting and silver stain PAGE to confirm expression and purification. Purified protein eluates were digested with trypsin for LC-MS/MS analysis. Samples were denatured and reduced in 2 M urea, 10 mM NH_4HCO_3, and 2 mM DTT for 30 min at 60°C and then alkylated with 2 mM iodoacetamide for 45 min at room temperature. Trypsin (Promega) was added at a 1:100 enzyme/substrate ratio and digested overnight at 37°C. Following digestion, samples were concentrated using C18 ZipTips (Millipore) according to the manufacturer's specifications. Peptides were resuspended in 15 μl of 4% formic acid and 3% ACN, and 1 to 2 μl of sample was loaded onto a 75-μm-ID column packed with 25 cm of Reprosil C18 1.9-μm, 120-Å particles (Dr. Maisch GmbH). Peptides were eluted into a Q-Exactive Plus (Thermo Fisher Scientific) mass spectrometer by gradient elution delivered by an Easy1200 nLC system (Thermo Fisher). The gradient was from 4.5% to 32% acetonitrile over 53 min. All MS spectra were collected with orbitrap detection, while the 20 most abundant ions were fragmented by higher energy collisional dissociation (HCD) and detected in the orbitrap. All data were searched against the Swiss-Prot Human protein sequences, combined with ZIKV sequences and GFP. Peptide and protein identification searches, as well as label-free quantitation, were performed using the MaxQuant data analysis algorithm, and all peptide and protein identifications were filtered to a 1% false-discovery rate (51, 52). SAINTq (53) was used to calculate the probability of bait-prey interactions for both Ugandan ZIKV capsid and French Polynesian ZIKV capsid against the negative controls, including GFP and empty vector, with protein intensities as input values. We applied a combined threshold of probability of interaction (AvgP) greater than 0.90 and a Bayesian false-discovery rate of less than 0.05.

Quantitative real-time reverse transcription-PCR (qRT-PCR). Total cellular RNA was isolated from Huh7 cells and NPCs using the RNeasy Mini kit (Qiagen). cDNA was synthesized with oligo$(dT)_{18}$ (Thermo Fisher Scientific) primers, random hexamer (Life Technologies) primers, and AMV reverse transcriptase (Promega). The cDNA was then used in SYBR green PCR master mix (Thermo Fisher Scientific) according to the manufacturer's instructions and analyzed by qPCR (Bio-Rad ABI 7900). The primers used for ASNS, CARS, SC35 1.7 (1.7 kb mRNA), GAPDH, HPRT1, LDHA, and 18S rRNA have been described previously (29). The additional primers used were as follows: ZIKV PRVABC59 forward primer, 5′-GAG ACG AGA TGC GGT ACA GG-3′; ZIKV PRVABC59 reverse primer, 5′-CGA CCG TCA GTT GAA CTC CA-3′; UPF1 forward primer, 5′-CTG CAA CGG ACG TGG AAA TAC-3′; UPF1 reverse primer, 5′-ACA GCC GCA GTT GTA GCA C-3′; DDIT3 forward primer, 5′- TG CTT CTC TGG CTT GGC TG-3′; DDIT3 reverse primer, 5′-GCT CTG GGA GGT GCT TGT GA-3′; GADD45A forward primer, 5′-GAG CTC CTG CTC TTG GAG AC-3′; GADD45A reverse primer, 5′-GCA GGA TCC TTC CAT TGA GA-3′; GADD45B forward primer, 5′-TGA CAA CGA CAT CAA CAT C-3′; GADD45B reverse primer, 5′-GTG ACC AGA GAC AAT GCA G-3′. The relative levels of each transcript were normalized by the delta threshold cycle method to the abundance of 18S rRNA or GAPDH, with mock-infected cells or vector-transfected cells set at 1.

Western blot analysis. Cells were lysed in RIPA lysis buffer (50 mM Tris-HCl [pH 8], 150 mM NaCl, 1% NP-40, 0.5% sodium deoxycholate, 0.1% SDS, supplemented with Halt protease inhibitor cocktail [Thermo Fisher Scientific]) to obtain whole-cell lysates or lysed using the NE-PER nuclear and cytoplasmic extraction kit (Thermo Fisher Scientific) to obtain cytoplasmic and nuclear fractions. Proteins were separated by SDS-PAGE and transferred to nitrocellulose membranes (Bio-Rad). Blots were incubated with the indicated primary antibody: anti-UPF3B (ab134566; Abcam), anti-UPF1 (12040; Cell Signaling Technology, Inc.), anti-ZIKV capsid (C) (GTX133304; GeneTex), anti-Flag (F7425; Sigma-Aldrich), anti-β-actin (A5316; Sigma-Aldrich), anti-ZIKV envelope (E) (GTX133314; GeneTex), anti-SP1 (sc-14027; Santa Cruz Biotechnology), anti-GAPDH (5174; Cell Signaling Technology, Inc.), anti-Myc tag (ab9106; Abcam), anti-Strep tag (ab18422, Abcam), and anti-p62 (ab56416, Abcam). Proteins were visualized by chemiluminescent detection with ECL and ECL Hyperfilm (Amersham). Differences in band intensity were quantified by densitometry using ImageJ.

Immunoprecipitations. Cells were lysed in either RIPA lysis buffer or IP lysis buffer (150 mM NaCl, 50 mM Tris [pH 7.4], 1 mM EDTA, 0.5% NP-40 substitute, supplemented with Halt protease inhibitor cocktail [Thermo Fisher Scientific]) at 4°C and passed through a G23 needle. Clarified lysates were immunoprecipitated with Flag M2 agarose (Sigma), anti-Myc tag (ab9106; Abcam), or normal rabbit IgG (sc-2027; Santa Cruz Biotechnology) overnight, washed in lysis buffer, and resuspended in Laemmli buffer for SDS-PAGE. Western blot analysis of immunoprecipitated proteins was performed as described above.

Immunofluorescence. Transfected Huh7-Lunet cells or infected NPCs were collected at 48 h and plated onto 22- by 22-mm no. 1.5 coverslips. Cells were fixed in 4% paraformaldehyde, permeabilized with 0.1% Triton X-100, and blocked in 3% bovine serum albumin. Cells were then immunostained with the indicated antibodies: anti-Strep Tag (ab184224; Abcam), anti-UPF1 (ab109363; Abcam), human anti-dengue virus (DENV) MAb 1.6D (Sharon Isern and Scott Michael, Florida Gulf Coast University), which recognizes the ZIKV envelope protein, anti-dsRNA MAb J2 (SCICONS), and the appropriate fluorophore-conjugated secondary antibodies. Coverslips were mounted onto glass slides using Vectashield mounting medium with DAPI (Vector Laboratories) and analyzed by fluorescence microscopy (Zeiss Axio

Observer ZI) or confocal microscopy (Zeiss LSM 880). For acquiring high-resolution images, cells were imaged on the Zeiss LSM 880 with Airyscan using a 20×/0.8 or 63×/1.4 M27 oil immersion objective. A total of 15 to 20 (20× objective) or 60 to 80 (63× objective) Z-slices were acquired every 0.88 μm or 0.15 μm, respectively. The resulting Z-stack was reconstructed and rendered in 3D using Imaris software (Bitplane). Viral dsRNA foci were reconstructed via the Imaris spot detection function, which provided an analysis of total number and mean volume of foci within a cell, for images acquired using the 20× objective. Strep-tagged ZIKV capsid, UPF1, and dsRNA channels acquired using the 63× objective were reconstructed using the Imaris surfaces package. The Imaris colocalization function was used to determine overlap of fluorescence. Thresholding for background fluorescence was determined by the Imaris automatic thresholding tool that utilizes the Costes approach (54). The thresholded Mander's correlation coefficient (MCC) measures the fraction of voxels with fluorescence positive for one channel that also contains fluorescence from another channel. The MCC is typically more appropriate for analysis of three-dimensional colocalization (55).

Statistical analysis. Statistical differences between groups were analyzed using either a two-tailed unpaired Student's *t* test or a two-tailed ratio paired Student's *t* test as stated in the figure legends. Hypergeometrical tests were used to calculate the probability of an overlap in gene dysregulation between ZIKV-infected NPCs and UPF1-depleted cells and to calculate the probability of ZIKV capsid bait-prey interactions. Data are represented as means plus standard errors of the means (SEM). Statistical significance was defined as follows: *, $P \leq 0.05$; **, $P \leq 0.01$; ***, $P \leq 0.001$; ****, $P \leq 0.0001$.

SUPPLEMENTAL MATERIAL

Supplemental material for this article may be found at https://doi.org/10.1128/mBio.02126-18.

FIG S1, PDF file, 0.2 MB.

FIG S2, PDF file, 0.4 MB.

FIG S3, PDF file, 10 MB.

ACKNOWLEDGMENTS

We thank all members of the Ott laboratory, as well as Roman Camarda, Marius Walter, and Anna Maurer for helpful discussions and advice throughout the preparation of the manuscript. We thank Chia-Lin Tsou, the Gladstone Stem Cell Core, and Meredith Calvert from the Gladstone Microscopy Core for technical assistance, and Ralf Bartenschlager (Heidelberg University), Lynne Maquat (University of Rochester), and Sharon Isern and Scott Michael (Florida Gulf Coast University) for reagents. We are grateful to Veronica Fonseca and Lauren Weiser for administrative support, John Carroll and Teresa Roberts for graphical design, and to Kathryn Claiborn, Eric Martens, and Gary Howard for editorial assistance.

This work was supported by NIH/NIAID F32AI112262 to P.S.S., NIH/NINDS R01 NS101996-01 to S.F., NIH/NIAID U19AI1186101 to N.J.K., DOD/DARPA HR0011-11-C-0094 (PROPHECY) to N.J.K., NIH/NIAID R01 AI097552 to M.O., BioFulcrum, and the James B. Pendleton Charitable Trust.

REFERENCES

1. Fauci AS, Morens DM. 2016. Zika virus in the Americas–yet another arbovirus threat. N Engl J Med 374:601–604. https://doi.org/10.1056/NEJMp1600297.
2. Cugola FR, Fernandes IR, Russo FB, Freitas BC, Dias JLM, Guimarães KP, Benazzato C, Almeida N, Pignatari GC, Romero S, Polonio CM, Cunha I, Freitas CL, Brandão WN, Rossato C, Andrade DG, Faria DdP, Garcez AT, Buchpigel CA, Braconi CT, Mendes E, Sall AA, Zanotto PM, Peron JPS, Muotri AR, Beltrão-Braga PCB. 2016. The Brazilian Zika virus strain causes birth defects in experimental models. Nature 534:267–271. https://doi.org/10.1038/nature18296.
3. Shao Q, Herrlinger S, Yang S, Lai F, Moore JM, Brindley MA, Chen J. 2016. Zika virus infection disrupts neurovascular development and results in postnatal microcephaly with brain damage. Development 143:4127–4136. https://doi.org/10.1242/dev.143768.
4. Souza BSF, Sampaio GLA, Pereira CS, Campos GS, Sardi SI, Freitas LAR, Figueira CP, Paredes BD, Nonaka CKV, Azevedo CM, Rocha VPC, Bandeira AC, Mendez-Otero R, Dos Santos RR, Soares MBP. 2016. Zika virus infection induces mitosis abnormalities and apoptotic cell death of human neural progenitor cells. Sci Rep 6:39775. https://doi.org/10.1038/srep39775.
5. Li C, Xu D, Xu Z, Ye Q, Hong S, Jiang Y, Liu X, Zhang N, Shi L, Qin C. 2016. Zika virus disrupts neural progenitor development and leads to microcephaly in mice. Cell Stem Cell 19:120–126. https://doi.org/10.1016/j.stem.2016.04.017.
6. Tang H, Hammack C, Ogden S, Wen Z, Qian X, Li Y, Yao B, Shin J, Zhang F, Lee E, Christian K, Didier R, Jin P, Song H, Ming G. 2016. Zika virus infects human cortical neural progenitors and attenuates their growth. Cell Stem Cell 18:587–590. https://doi.org/10.1016/j.stem.2016.02.016.
7. Rasmussen SA, Jamieson DJ, Honein MA, Petersen LR. 2016. Zika virus and birth defects–reviewing the evidence for causality. N Engl J Med 374:1981–1987. https://doi.org/10.1056/NEJMsr1604338.
8. Harris E, Holden KL, Edgil D, Polacek C, Clyde K. 2006. Molecular biology of flaviviruses. Novartis Found Symp 277:253.
9. Lindenbach BD, Rice CM. 2003. Molecular biology of flaviviruses. Adv Virus Res 59:23–61. https://doi.org/10.1016/S0065-3527(03)59002-9.
10. Oliveira ERA, Mohana-Borges R, de Alencastro RB, Horta BAC. 2017. The flavivirus capsid protein: structure, function and perspectives towards drug design. Virus Res 227:115–123. https://doi.org/10.1016/j.virusres.2016.10.005.
11. den Boon JA, Diaz A, Ahlquist P. 2010. Cytoplasmic viral replication complexes. Cell Host Microbe 8:77–85. https://doi.org/10.1016/j.chom.2010.06.010.

12. Colpitts TM, Barthel S, Wang P, Fikrig E. 2011. Dengue virus capsid protein binds core histones and inhibits nucleosome formation in human liver cells. PLoS One 6:e24365. https://doi.org/10.1371/journal.pone.0024365.
13. Slomnicki LP, Chung DH, Parker A, Hermann T, Boyd NL, Hetman M. 2017. Ribosomal stress and Tp53-mediated neuronal apoptosis in response to capsid protein of the Zika virus. Sci Rep 7:1–15.
14. Tsuda Y, Mori Y, Abe T, Yamashita T, Okamoto T, Ichimura T, Moriishi K, Matsuura Y. 2006. Nucleolar protein B23 interacts with Japanese encephalitis virus core protein and participates in viral replication. Microbiol Immunol 50:225–234. https://doi.org/10.1111/j.1348-0421.2006.tb03789.x.
15. Xu Z, Hobman TC. 2012. The helicase activity of DDX56 is required for its role in assembly of infectious West Nile virus particles. Virology 433:226–235. https://doi.org/10.1016/j.virol.2012.08.011.
16. Rawlinson SM, Moseley GW. 2015. The nucleolar interface of RNA viruses. Cell Microbiol 17:1108–1120. https://doi.org/10.1111/cmi.12465.
17. Peccarelli M, Kebaara BW. 2014. Regulation of natural mRNAs by the nonsense-mediated mRNA decay pathway. Eukaryot Cell 13:1126–1135. https://doi.org/10.1128/EC.00090-14.
18. Hug N, Longman D, Cáceres JF. 2016. Mechanism and regulation of the nonsense-mediated decay pathway. Nucleic Acids Res 44:1483–1495. https://doi.org/10.1093/nar/gkw010.
19. Han X, Wei Y, Wang H, Wang F, Ju Z, Li T. 2018. Nonsense-mediated mRNA decay: a 'nonsense' pathway makes sense in stem cell biology. Nucleic Acids Res 46:1038–1051. https://doi.org/10.1093/nar/gkx1272.
20. Silver DL, Watkins-Chow DE, Schreck KC, Pierfelice TJ, Larson DM, Burnetti AJ, Liaw H, Myung K, Walsh CA, Gaiano N, Pavan WJ. 2010. The exon junction complex component Magoh controls brain size by regulating neural stem cell division. Nat Neurosci 13:551–558. https://doi.org/10.1038/nn.2527.
21. Mao H, Pilaz L, McMahon JJ, Golzio C, Wu D, Shi L, Katsanis N, Silver DL. 2015. Rbm8a haploinsufficiency disrupts embryonic cortical development resulting in microcephaly. J Neurosci 35:7003–7018. https://doi.org/10.1523/JNEUROSCI.0018-15.2015.
22. Mao H, McMahon JJ, Tsai Y, Wang Z, Silver DL. 2016. Haploinsufficiency for core exon junction complex components disrupts embryonic neurogenesis and causes p53-mediated microcephaly. PLoS Genet 12:e1006282. https://doi.org/10.1371/journal.pgen.1006282.
23. Kurosaki T, Maquat LE. 2016. Nonsense-mediated mRNA decay in humans at a glance. J Cell Sci 129:461–467. https://doi.org/10.1242/jcs.181008.
24. Serquiña AKP, Das SR, Popova E, Ojelabi OA, Roy CK, Göttlinger HG. 2013. UPF1 is crucial for the infectivity of human immunodeficiency virus type 1 progeny virions. J Virol 87:8853–8861. https://doi.org/10.1128/JVI.00925-13.
25. Molleston JM, Cherry S. 2017. Attacked from all sides: RNA decay in antiviral defense. Viruses 9:2. https://doi.org/10.3390/v9010002.
26. Balistreri G, Bognanni C, Mühlemann O. 2017. Virus escape and manipulation of cellular nonsense-mediated mRNA decay. Viruses 9:24. https://doi.org/10.3390/v9010024.
27. Rigby RE, Rehwinkel J. 2015. RNA degradation in antiviral immunity and autoimmunity. Trends Immunol 36:179–188. https://doi.org/10.1016/j.it.2015.02.001.
28. Balistreri G, Horvath P, Schweingruber C, Zünd D, McInerney G, Merits A, Mühlemann O, Azzalin C, Helenius A. 2014. The host nonsense-mediated mRNA decay pathway restricts mammalian RNA virus replication. Cell Host Microbe 16:403–411. https://doi.org/10.1016/j.chom.2014.08.007.
29. Ramage HR, Kumar GR, Verschueren E, Johnson JR, Von Dollen J, Johnson T, Newton B, Shah P, Horner J, Krogan NJ, Ott M. 2015. A combined proteomics/genomics approach links hepatitis C virus infection with nonsense-mediated mRNA decay. Mol Cell 57:329–340. https://doi.org/10.1016/j.molcel.2014.12.028.
30. Tani H, Imamachi N, Salam KA, Mizutani R, Ijiri K, Irie T, Yada T, Suzuki Y, Akimitsu N. 2012. Identification of hundreds of novel UPF1 target transcripts by direct determination of whole transcriptome stability. RNA Biol 9:1370–1379. https://doi.org/10.4161/rna.22360.
31. Weischenfeldt J, Damgaard I, Bryder D, Theilgaard-Mönch K, Thoren LA, Nielsen FC, Jacobsen SEW, Nerlov C, Porse BT. 2008. NMD is essential for hematopoietic stem and progenitor cells and for eliminating by-products of programmed DNA rearrangements. Genes Dev 22:1381–1396. https://doi.org/10.1101/gad.468808.
32. Li T, Shi Y, Wang P, Guachalla LM, Sun B, Joerss T, Chen Y, Groth M, Krueger A, Platzer M, Yang Y, Rudolph KL, Wang Z. 2015. Smg6/Est1 licenses embryonic stem cell differentiation via nonsense-mediated mRNA decay. EMBO J 34:1630–1647. https://doi.org/10.15252/embj.201489947.
33. Brazão TF, Demmers J, van IJcken W, Strouboulis J, Fornerod M, Romão L, Grosveld FG. 2012. A new function of ROD1 in nonsense-mediated mRNA decay. FEBS Lett 586:1101–1110. https://doi.org/10.1016/j.febslet.2012.03.015.
34. Chan W, Huang L, Gudikote JP, Chang Y, Imam JS, MacLean JA, Wilkinson MF. 2007. An alternative branch of the nonsense-mediated decay pathway. EMBO J 26:1820–1830. https://doi.org/10.1038/sj.emboj.7601628.
35. Nelson JO, Moore KA, Chapin A, Hollien J, Metzstein MM. 2016. Degradation of Gadd45 mRNA by nonsense-mediated decay is essential for viability. Elife 5:e12876. https://doi.org/10.7554/eLife.12876.
36. Jauhiainen A, Thomsen C, Strömbom L, Grundevik P, Andersson C, Danielsson A, Andersson MK, Nerman O, Rörkvist L, Ståhlberg A, Åman P. 2012. Distinct cytoplasmic and nuclear functions of the stress induced protein DDIT3/CHOP/GADD153. PLoS One 7:e33208. https://doi.org/10.1371/journal.pone.0033208.
37. Salvador JM, Brown-Clay JD, Fornace AJ. 2013. Gadd45 in stress signaling, cell cycle control, and apoptosis. Adv Exp Med Biol 793:1–19. https://doi.org/10.1007/978-1-4614-8289-5_1.
38. Gehring NH, Lamprinaki S, Kulozik AE, Hentze MW. 2009. Disassembly of exon junction complexes by PYM. Cell 137:536–548. https://doi.org/10.1016/j.cell.2009.02.042.
39. Chamieh H, Ballut L, Bonneau F, Le Hir H. 2008. NMD factors UPF2 and UPF3 bridge UPF1 to the exon junction complex and stimulate its RNA helicase activity. Nat Struct Mol Biol 15:85–93. https://doi.org/10.1038/nsmb1330.
40. Varsally W, Brogna S. 2012. UPF1 involvement in nuclear functions. Biochem Soc Trans 40:778–783. https://doi.org/10.1042/BST20120052.
41. Klema VJ, Padmanabhan R, Choi KH. 2015. Flaviviral replication complex: coordination between RNA synthesis and 5′-RNA capping. Viruses 7:4640–4656. https://doi.org/10.3390/v7082837.
42. Maisel M, Herr A, Milosevic J, Hermann A, Habisch H, Schwarz S, Kirsch M, Antoniadis G, Brenner R, Hallmeyer-Elgner S, Lerche H, Schwarz J, Storch A. 2007. Transcription profiling of adult and fetal human neuroprogenitors identifies divergent paths to maintain the neuroprogenitor cell state. Stem Cells 25:1231–1240. https://doi.org/10.1634/stemcells.2006-0617.
43. Li H, Saucedo-Cuevas L, Regla-Nava J, Chai G, Sheets N, Tang W, Terskikh A, Shresta S, Gleeson J. 2016. Zika virus infects neural progenitors in the adult mouse brain and alters proliferation. Cell Stem Cell 19:593–598. https://doi.org/10.1016/j.stem.2016.08.005.
44. Nickless A, Bailis JM, You Z. 2017. Control of gene expression through the nonsense-mediated RNA decay pathway. Cell Biosci 7:1–12. https://doi.org/10.1186/s13578-017-0153-7.
45. Cortese M, Goellner S, Acosta EG, Neufeldt CJ, Oleksiuk O, Lampe M, Haselmann U, Funaya C, Schieber N, Ronchi P, Schorb M, Pruunsild P, Schwab Y, Chatel-Chaix L, Ruggieri A, Bartenschlager R. 2017. Ultrastructural characterization of Zika virus replication factories. Cell Rep 18:2113–2123. https://doi.org/10.1016/j.celrep.2017.02.014.
46. Grant A, Ponia SS, Tripathi S, Balasubramaniam V, Miorin L, Sourisseau M, Schwarz MC, Sánchez-Seco MP, Evans MJ, Best SM, García-Sastre A. 2016. Zika virus targets human STAT2 to inhibit type I interferon signaling. Cell Host Microbe 19:882–890. https://doi.org/10.1016/j.chom.2016.05.009.
47. von Mikecz A. 2006. The nuclear ubiquitin-proteasome system. J Cell Sci 119:1977–1984. https://doi.org/10.1242/jcs.03008.
48. Freire JM, Veiga AS, Conceição TM, Kowalczyk W, Mohana-Borges R, Andreu D, Santos NC, Da Poian AT, Castanho MARB. 2013. Intracellular nucleic acid delivery by the supercharged dengue virus capsid protein. PLoS One 8:e81450. https://doi.org/10.1371/journal.pone.0081450.
49. HD iPSC Consortium. 2017. Developmental alterations in Huntington's disease neural cells and pharmacological rescue in cells and mice. Nat Neurosci 20:648–660. https://doi.org/10.1038/nn.4532.
50. Jäger S, Gulbahce N, Cimermancic P, Kane J, He N, Chou S, D'Orso I, Fernandes J, Jang G, Frankel AD, Alber T, Zhou Q, Krogan NJ. 2011. Purification and characterization of HIV-human protein complexes. Methods 53:13–19. https://doi.org/10.1016/j.ymeth.2010.08.007.
51. Cox J, Hein MY, Luber CA, Paron I, Nagaraj N, Mann M. 2014. Accurate proteome-wide label-free quantification by delayed normalization and maximal peptide ratio extraction, termed MaxLFQ. Mol Cell Proteomics 13:2513–2526. https://doi.org/10.1074/mcp.M113.031591.
52. Cox J, Mann M. 2008. MaxQuant enables high peptide identification rates, individualized p.p.b.-range mass accuracies and proteome-wide

protein quantification. Nat Biotechnol 26:1367–1372. https://doi.org/10.1038/nbt.1511.

53. Teo G, Koh H, Fermin D, Lambert J, Knight JDR, Gingras A, Choi H. 2016. SAINTq: scoring protein-protein interactions in affinity purification – mass spectrometry experiments with fragment or peptide intensity data. Proteomics 16:2238–2245. https://doi.org/10.1002/pmic.201500499.
54. Costes SV, Daelemans D, Cho EH, Dobbin Z, Pavlakis G, Lockett S. 2004. Automatic and quantitative measurement of protein-protein colocalization in live cells. Biophys J 86:3993–4003. https://doi.org/10.1529/biophysj.103.038422.
55. Dunn KW, Kamocka MM, McDonald JH. 2011. A practical guide to evaluating colocalization in biological microscopy. Am J Physiol Cell Physiol 300:C723–C742. https://doi.org/10.1152/ajpcell.00462.2010.
56. Paul LM, Carlin ER, Jenkins MM, Tan AL, Barcellona CM, Nicholson CO, Michael SF, Isern S. 2016. Dengue virus antibodies enhance Zika virus infection. Clin Transl Immunol 5:e117. https://doi.org/10.1038/cti.2016.72.